Density Functional Theory Studies of Ethanol Decomposition on Rh(211)

ARTICLE *in* THE JOURNAL OF PHYSICAL CHEMISTRY C · OCTOBER 2011

Impact Factor: 4.77 · DOI: 10.1021/jp206837z

THE JOURNAL OF PHYSICAL CHEMISTRY C

ARTICLE

pubs.acs.org/JPCC

Density Functional Theory Studies of Ethanol Decomposition on Rh(211)

Jia Zhang,[†] X.-M. Cao,[‡] P. Hu,[‡,§] Ziyi Zhong,[∥] Armando Borgna,[∥] and Ping Wu*[,†,⊥]

[†]Institute of High Performance Computing, 1 Fusionopolis Way #16-16 Connexis Singapore 138632

[‡]State Key Laboratory of Chemical Engineering, Centre for Computational Chemistry and Research Institute of Industrial Catalysis, East China University of Science and Technology, Shanghai 200237, P.R. China

[§]School of Chemistry and Chemical Engineering, Queen's University of Belfast, Belfast, BT9 5AG, U.K.

[∥]Institute of Chemical Engineering and Sciences, 1 Pesek Road, Jurong Island, Singapore 627833

Supporting Information

ABSTRACT: Density functional theory calculations were carried out to examine the mechanism of ethanol decomposition on the Rh(211) surface. We found that there are two possible decomposition pathways: (1) $CH_3CH_2OH \rightarrow CH_3CHOH \rightarrow CH_3COH \rightarrow CH_3CO \rightarrow CH_3 + CO \rightarrow CH_2 + CO \rightarrow CH + CO \rightarrow C + CO$ and (2) $CH_3CH_2OH \rightarrow CH_3CHOH \rightarrow CH_3COH \rightarrow CH_2COH \rightarrow CHCOH \rightarrow CHCO \rightarrow CH + CO \rightarrow C + CO$. Both pathways have a common intermediate of CH_3COH, and the key step is the formation of CH_3CHOH species. According to our calculations, the mechanism of ethanol decomposition on Rh(211) is totally different from that on Rh(111): the reaction proceeds via CH_3COH rather than an oxametallacycle species ($-CH_2CH_2O-$ for Rh(111)), which implies that the decomposition process is structure sensitive. Further analyses on electronic structures revealed that the preference of the initial $C_\alpha-H$ path is mainly due to the significant reduction of d-electron energy in the presence of the transition state (TS) complex, which may stabilize the TS−surface system. The present work first provides a clear picture for ethanol decomposition on stepped Rh(211), which is an important first step to completely understand the more complicated reactions, like ethanol steam reforming and electrooxidation.

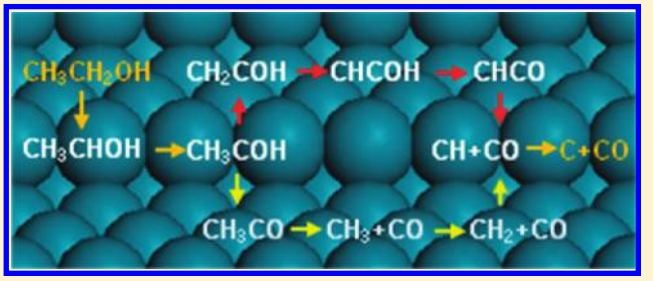

1. INTRODUCTION

Ethanol, as an alternative fuel, to be used either to produce hydrogen or as a direct ethanol fuel cell, has drawn much attention due to its unique advantages, such as high hydrogen content and nontoxicity. In industry, steam reforming is widely used to convert ethanol to CO and H_2, in which ethanol decomposition is one of the key steps. Recently, a number of studies have revealed that ethanol conversion and hydrogen yield largely depend on catalysts and reaction conditions.[1,2] Thus, selecting a suitable and durable catalyst to selectively trigger desirable reactions becomes a crucial issue in the entire thermochemical process. Indeed, one of the key factors to determine the suitability of a catalyst is the capability to activate adsorbed molecules,[4] e.g., selective cleavage of the C−C bond in ethanol decomposition.[5] In the past, the ethanol adsorption and dissociation have been investigated on many transition metal surfaces, like Pd(111), Pt(111), Rh(111), and Ni(111), by various surface science techniques and ab initio calculations.[6−14] People found that Rh exhibits the best catalytic activity for C−C bond rupture and generates less carbon deposits as compared to Ni.[1−3] Temperature-programmed desorption (TPD) and high-resolution electron energy loss spectroscopy (HREELS) studies of ethanol decomposition on Rh(111) indicated that a surface oxametallacycle is a stable intermediate by sequential hydrogen abstraction from the hydroxyl and methyl group.[7] In addition, the further mechanism investigations by density functional theory (DFT) calculations revealed that the β-dehydrogenation of CH_3CH_2O is the rate-determining step in the course of ethanol decomposition on Rh(111).[12,13]

To further improve the catalytic performance, at present, the experimental efforts are focused on two areas: modifying surface composition and crystallographic structure. In the first case, a second metal, like Au, Ni, and Pt, is introduced into the Rh matrix to form an alloy catalyst.[15−19] The bimetallic catalyst combines the advantage of each of its constituents and has higher possibilities to increase catalytic activity and selectivity. TPD experiments and infrared spectroscopy revealed that the addition of Au enhances the rate of ethanol oxidation.[15] In addition, studies on Rh−Pt bimetallic catalysts indicated that Rh facilitates a direct splitting of the C−C bond, while Pt facilities ethanol dehydrogenation;[16,17] thus, the cooperative effect of Rh and Pt makes the catalyst more efficient. As for the influence of surface

Received: July 18, 2011
Revised: September 26, 2011
Published: September 28, 2011

dx.doi.org/10.1021/jp206837z | J. Phys. Chem. C 2011, 115, 22429–22437

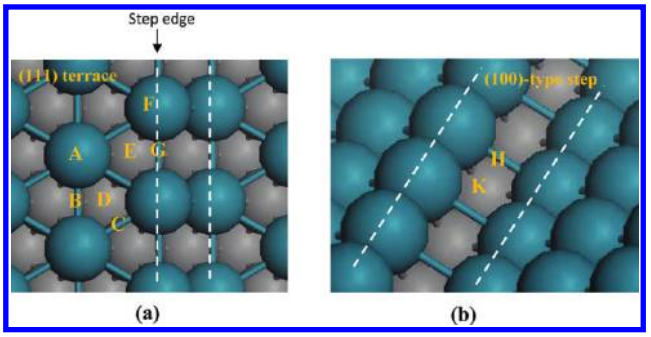

Figure 1. Schematic illustration of considered adsorption sites on the Rh(211) surface. (a) Top view of the Rh(211) surface, including the (111) terrace and (100)-type step. The step edge is indicated by the arrow. A−E represent adsorption sites on the (111) terrace; i.e., A is the *t*-top site, B is the *t*-bridge site, C is the t_e-bridge site (the subscript *e* means the Rh atom on the step edge is involved), D is the *t*-fcc site, and E is the *t*-hcp site, where the tilted *t* represents terrace. F and G correspond to adsorption sites on the step edge: F is the *e*-top site, and G is the *e*-bridge site, where the tilted *e* stands for step edge. (b) The (100)-type step. H and K denote adsorption sites on step: H is the *s*-bridge site, and K is the *s*-hollow site, where the tilted *s* represents step.

structure on catalytic properties, it is long believed that the surface defect plays an important role in determining reaction pathways and thus eventually affects reaction activity and selectivity. A number of instances have proved that the catalytic properties are surface-sensitive for some metals.[20−26] The stepped Pt surfaces, (335), (557), and (331), exhibit unusual activity for C−C bond cleavage in ethanol.[20−22] Also, on the Pd(110) surface ethanol decomposition occurs via acetyl to the methyl group,[25] but it proceeds via acetyl to a ketene species by dehydrogenation on Pd(111).[27]

In the past, research on the Rh catalyst focused on the Rh(111) surface either for ethanol decomposition or for the reverse reaction to form ethanol. Although step is the most common defect for the nanosized metal catalyst used in reality, studies in this area are limited. Resta et al. compared the ethanol dehydrogenation on Rh(111) and Rh(553) surfaces by using high-resolution core level photoemission and DFT calculations and found that the Rh(553) surface enhances dehydrogenation as compared to the Rh(111) surface.[28] Yet, to date, the actual mechanism of ethanol decomposition on the stepped surface is still unclear: (1) What is the most favorable reaction pathway? (2) What is the key step? (3) How does the surface facet influence the catalytic reaction? To tackle these puzzles, we investigated the dissociation behavior of ethanol on the stepped Rh(211) surface in this work. The Rh(211) surface having the (100)-type step is generally quite active in catalytic reactions.[29,30] By mapping out the whole reaction network and the rate-limiting step, we aim to get a clear picture of the ethanol dissociation on the stepped Rh(211) surface. The findings may provide useful information for further studying steam reforming of ethanol on a Rh-based catalyst.

2. COMPUTATIONAL METHODS

DFT calculations were performed using the Vienna Ab initio Simulation package (VASP),[31] in which a plane-wave basis set is used. The electron−ion interaction was modeled by the projector-augmented wave (PAW) method.[32,33] The (PW91) form of the generalized-gradient approximation (GGA) was used for the exchange and correlation functional.[34] The plane-wave cutoff energy was set to 400 eV, and 8 × 8 × 8 and 2 × 3 × 1 k-point mesh with Monkhorst−Pack scheme were used for bulk and surface calculations, respectively. The calculated lattice constant is 3.841 Å for Rh bulk, which is in good agreement with the experimental and theoretical values of 3.797[35] and 3.843 Å,[36] respectively. The $p(2 \times 3)$ Rh(211) surface is simulated using a slab supercell approach with periodic boundary conditions. The slab contained four layers of metal atoms of which the bottom two layers are frozen and the top two metal layers are allowed to move freely. We used a vacuum region of 15 Å, which is large enough to avoid interactions between adsorbates and slab images. The vacuum size, cutoff energy, and k-point mesh were tested for convergence. All transition states (TSs) were located using the constrained minimization technique.[37]

In this work, we studied the adsorption of various reactants, intermediates, and products on the Rh(211) surface. The adsorption energy is defined as $E_{ad} = E_{slab+A} - E_{slab} - E_A$, where the E_{slab+A} is the total energy of the slab with the intermediate; E_{slab} is the energy of the clean Rh(211) surface; and E_A is the energy of the gas-phase adsorbate A. Also, the reaction energy is defined as $\Delta E = E_{product} - E_{reactant}$. Herein, spin-polarized calculations were carried out for gas-phase radical species derived from ethanol. By definition, a negative value corresponds to exothermic adsorption.

In addition, to build the energy profile of the whole reaction, we calculated the relative energy (E_r) of adsorbed intermediates and transition states with reference to the gas-phase ethanol plus clean surface, which is expressed as $E_r = E_{slab+A} + nE_{H+slab} - (n + 1)E_{slab} - E_{ethanol}$, where E_{slab+A}, E_{H+slab}, E_{slab}, and $E_{ethanol}$ represent the total energies of adsorbed intermediates, adsorbed H atom, clean Rh(211) surface, and gas-phase ethanol, respectively. *n* is the number of the removed H atoms from ethanol in dehydrogenation reactions. For example, for the intermediate CH_3CHOH, *n* is equal to 1.

The DFT calculations on gas-phase ethanol indicated that the C−C, C−O bonds and the angle C−C−O are 1.518 Å, 1.439 Å, and 108.6°, respectively, which are in good agreement with previous experimental (1.51 Å, 1.43 Å, and 108°)[38] and theoretical values (1.52 Å, 1.43 Å, and 113°).[5]

3. RESULTS AND DISCUSSION

3.1. Adsorption of Reactants and Intermediates on Rh(211). As the starting point, the adsorption behavior of ethanol as well as ethanol-derived intermediates on the stepped Rh(211) surface was investigated in this work. Here, nine possible adsorption sites were considered. As shown in Figure 1, molecular species are likely to adsorb on the surface at the top site (-top), bridge site (-bri), or hollow site (-hol). All selected adsorption sites are categorized into three groups, including five sites on the (111) terrace (labeled as *t*-fcc, *t*-hcp, *t*-bri, t_e-bri, and *t*-top), two sites on the step-edge (labeled as *e*-top and *e*-bri), and two sites on the (100)-type step (labeled as *s*-bri and *s*-hol). We summarized the adsorption site, corresponding adsorption energy (E_{ad}), as well as important geometric parameters at equilibrium in Table 1. Results showed that ethanol and most ethanol-derived species always prefer to adsorb on step-edge sites. For example, for the ethanol molecule, the most stable chemisorption site moves to the *e*-top site on the step-edge of Rh(211), although it was found to be the *t*-top site when ethanol is adsorbed on Rh(111).[13,39] The ethanol interacts with the Rh-

Table 1. Adsorption Energies and Geometry Parameters of Some Important Intermediates for Ethanol Decomposition on Rh(211)

species	E_{ad} (eV)	$d_{C(\alpha)-Rh}$ (Å)	$d_{C(\beta)-Rh}$ (Å)	d_{O-Rh} (Å)	adsorption site
CH_3CH_2OH	−0.62			2.257	*e*-top via O
CH_3CHOH	−2.22	2.066		2.247	*e*-top via C_α, C−O bond parallel (slightly tilted) to the Rh-step
CH_3CH_2O	−2.89			2.066/2.073	*e*-bri via O
CH_3COH	−3.40	2.068/2.071			*e*-bri via C_α
CH_2COH	−3.63	1.989	2.164		metallacycle species via C_α and C_β at Rh-step
CH_3CO	−2.83	1.949		2.121	oxametallacycle species via C_α and O at Rh-step
CH_2CO	−1.61	1.998	2.100		metallacycle species via C_α and C_β at Rh-step
CHCOH	−3.26	1.978	2.083/2.043		*e*-bri via C_β, near top site of the terrace via C_α
CHCO	−3.73	2.076	2.044/2.035		*e*-bri via C_β, near top site of the terrace via C_α
COH	−4.61	1.918/1.918			*e*-bri via C
CH_4	−0.11	2.677			*e*-top via C
CH_3	−2.13	2.066			*e*-top via C
CH_2	−4.49	2.021/2.024			*e*-bri via C
CH	−6.90	2.103/2.104/2.108/2.109			*s*-hol on (100)-type step
CO	−2.13	2.012/2.014			*e*-bri via C
OH	−3.60			2.096/2.097	*e*-bri via O
O	−5.71			1.897/1.901	*e*-bri
C	−8.03	1.988/1.989/2.015/2.015			*s*-hol on (100)-type step
H	−2.87	d_{Rh-H} = 1.763/1.764			*e*-bri

step through O (O−Rh = 2.23 Å) and the adsorption energy of −0.62 eV. This is in good agreement with the previous calculations done by Kapur and co-workers.[39] We found that the steps improve E_{ad} (C_2H_5OH) by 0.17 and 0.29 eV relative to the *t*-top site on Rh(211) and on Rh(111), respectively. Actually, the influence of surface defects on adsorption strength is not limited to ethanol but also for other species and metal surfaces, like CH_3−Pt(111)/(211) adsorption systems.[30] This kind of high activity for step metal atoms can be attributed to their lower coordination number (CN) as compared to the flat surface atom, for example, on Rh(111) CN = 9, while on Rh(211)-step CN = 7, thus the extra dangling bonds induced by defect make the surface step more active in catalytic reactions. In addition, we noticed that the binding of ethanol at the *t*-top site on the Rh(211) terrace (−0.45 eV) is more stable than that on the flat Rh(111) surface (−0.33 eV), which can be interpreted as due to the coverage effect. Herein, we modeled the flat Rh(111) surface using a p(2 × 2) slab, corresponding to a higher coverage of 1/4 ML, while the Rh-step was modeled by a (2 × 3) Rh(211) slab, resulting in a lower coverage of 1/6 ML. Thus, the steric repulsion in a higher coverage slightly weakens the molecule−surface interaction.[40]

For the ethanol dissociation, the first and foremost step is dehydrogenation. We compared the adsorption energy of H at various adsorption sites and found that the two edge adsorption sites (*e*-top and *e*-bri) have quite different selectivity to H. For the top site, the H atom has almost the same chemisorption energy on the Rh-step and (111) terrace (the energy difference is 0.05 eV), which is consistent with the previous calculations of Liu and Hu.[30] However, the *e*-bri site (E_{ad} = −2.87 eV) significantly lowers the E_{ad}(H) by 0.37 eV relative to the *e*-top site. By removing H from the α-C/β-C atom as well as breaking the C−C bond, various C_1 and C_2 surface species can be obtained. With the increase in the valency of the C atom (due to the continuous removal of H atoms), it can be seen that the adsorption site shifts from *e*-top (monovalent C) to *e*-bridge (divalent C) and finally to hollow site (trivalent C). For example, both 1-hydroxyethyl (CH_3CHOH) and 1-hydroxyethylidene (CH_3COH) bind to the Rh surface via α-C; however, the most stable adsorption site moves from *e*-top to *e*-bridge due to the changes in C valency. In addition, the metallacycle species can be observed when at least two of the three heavy atoms (α-C, β-C, and O) are unsaturated. Here, we take ketene (CH_2CO) as an example as it is an important intermediate on the reaction pathway. We found that there are two adsorption modes that can result in stable binding of ketene to Rh(211). In the first mode, the ketene interacts with Rh(211) through α-C, β-C, and O, and the adsorption sites are close to the Rh-edge; i.e., α-C sits on *e*-bri, β-C is near *e*-top, and O is on *t*-top. This configuration is very similar to the one that Kapur et al. reported in their recent paper, which leads to a E_{ad}(CH_2CO) equal to −1.59 eV, close to the literature value of −1.71 eV.[39] In fact, another adsorption mode is even more stable (E_{ad}(CH_2CO) = −1.61 eV), in which both of the two adsorption sites are on the Rh-edge and a Rh−C_α−C_β−Rh metallacycle is formed. In fact, the two adsorption modes stretch the C−C double bond (1.313 Å in gas-phase CH_2CO) and make it have a C−C single bond character with d_{c-c} = 1.424 and 1.465 Å, respectively.

There are a number of reaction intermediates in the entire process of ethanol decomposition. Compared with the available literature data, our present computational results are in excellent agreement with them. All optimized configurations are shown in Figure S1 in the Supporting Information.

3.2. Reaction Network of Ethanol Decomposition on Rh(211). The decomposition of ethanol refers to several bond cleavages, including the C−H, C−C, C−O, and O−H bonds. In this section, we investigated all possible bond scissions step by step. The reaction barriers (E_a) at each step are compared, and the reaction undergoes the minimization energy path until the final C_1 species is reached.

3.2.1. Bond Scission in Ethanol (CH_3CH_2OH). We start from the adsorbed ethanol and identify four possible pathways, i.e.,

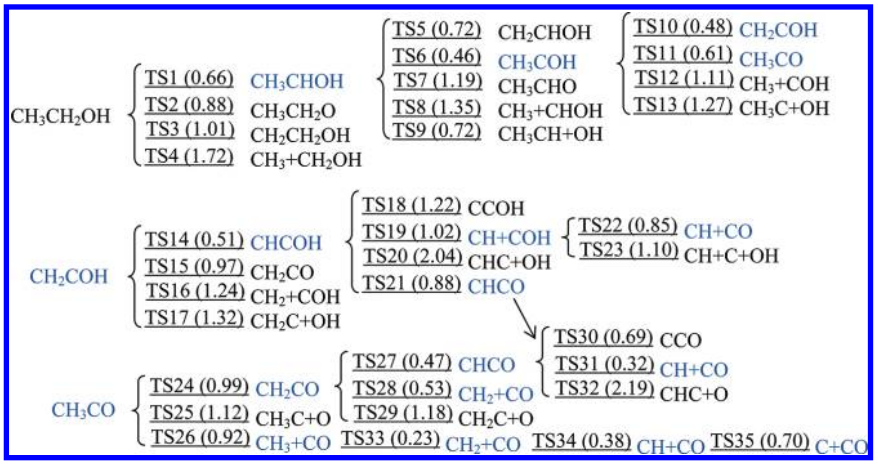

Figure 2. Reaction network and energy barriers (unit, eV) for ethanol decomposition on Rh(211). For clarity, H atoms produced in the course of ethanol decomposition were omitted. The blue means the most likely intermediates produced in the decomposition process.

C−H, C−C, and O−H bond breaking first, in which the C−H paths include α-dehydrogenation to produce CH_3CHOH and β-dehydrogenation to generate CH_2CH_2OH. At the initial bond breaking of ethanol, as shown in Figure 2, the most difficult reaction pathway is C−C bond scission (E_a = 1.72 eV), followed by β-hydrogen elimination with a high-energy barrier over 1 eV (E_a = 1.01 eV). Among these four reaction pathways, the C_α−H path is the most likely reaction pathway with the lowest energy barrier (E_a) of 0.66 eV. At the transition state of this step (TS1), the C_α−H bond is breaking on a Rh atom at the step edge with a C−H distance of 1.582 Å. The C−O bond (1.452 Å, closer to the d_{C-O} = 1.439 Å in ethanol) is almost parallel (slightly tilted) to the Rh-step, and C_α−Rh and O−Rh distances are 2.200 and 2.365 Å, respectively. It is interesting to note that on Rh (211) the C_α−H path is more facile compared to the O−H path where ethoxy (CH_3CH_2O) is produced. The energy barrier for α-dehydrogenation is lower than that for hydroxyl dehydrogenation (E_a = 0.88 eV) by 0.22 eV. This point is quite different from previous findings on Rh(111), on which the ethoxide (yielded via the O−H path) is usually considered as a stable intermediate, and the further β-H abstraction leads to oxametallacycle intermediates ($-CH_2CH_2O-$).[7] To verify the preference of the O−H path on Rh(111), we investigated the two key pathways on it, i.e., the C_α−H bond and O−H bond scission in ethanol. The calculations indicated that the energy barrier of the O−H path is 0.78 eV, 0.14 eV lower than that of the α-dehydrogenation path (E_a = 0.92 eV). That result is consistent with the recent DFT calculations by Li et al., in which the reaction barriers on Rh(111) for breaking O−H and α-C−H bonds are 0.75 eV (17.3 kcal/mol) and 1.44 eV (33.3 kcal/mol), respectively.[13] Compared to the Rh(111) surface, the initial bond breaking of ethanol on Rh(211) is more like that on Pt(111) and Pt(211), where α-dehydrogenation to yield 1-hydroxyethyl (CH_3CHOH) is favorable.[26,41] Indeed, the initial decomposition behavior of ethanol on rhodium is surface-sensitive. The Rh-step in the Rh(211) surface reverses the sequence of initial bond breaking and thus changes the entire reaction mechanism relative to Rh(111).

3.2.2. Bond Scission in 1-Hydroxyethyl (CH_3CHOH), 1-Hydroxyethylidene (CH_3COH), Acetyl (CH_3CO), and 1-Hydroxyvinyl (CH_2COH). For the further degradation of CH_3CHOH, there are five distinct reaction paths (C_α−H, C_β−H, O−H, C−C, and C−O) to be considered. Judging from energy barriers in Figure 2, we found that in the increasing order of the reaction barriers for bond breaking we have C_α−H (0.46 eV) < C_β−H (0.72 eV) = C−O (0.72 eV) < O−H (1.19 eV) < C−C (1.35 eV). It can be seen that the α-H removal is the most favorable reaction pathway. The C_α−H bond is broken over the Rh-step edge with H and α-C separately adsorbing on the two neighboring edge-Rh-atoms. The dissociating C_α−H bond distance is 1.772 Å, while the C−O bond shrinks to 1.356 Å with more double bond character. In addition, we found that a high energy barrier of 1.19 eV is obtained for the O−H bond cleavage, and thus it seems that acetaldehyde (CH_3CHO) is difficult to be formed in the course of ethanol dissociation on rhodium. This is the same as the general findings on Rh(111) that acetaldehyde is excluded in the ethanol decomposition process because no methane is detected in the TPD spectra, while the oxametallacycle species ($-CH_2CH_2O-$) is suggested as a plausible intermediate by several experiments and DFT calculations.[7,12−14,16] However, on Rh(211) the dissociation channel to obtain CH_2CH_2O is abandoned. In fact, on the stepped Rh(211) surface, the formation of 1-hydroxyethylidene (CH_3COH) is more favorable according to our calculations. Besides, Kapur and co-workers reported that CO insertion into methylene (CH_2) can produce ethanol on Rh(211) through the CH_3COH intermediate.[39] Therefore, for either the forward reaction (ethanol decomposition) or the reverse reaction (ethanol synthesis), CH_3COH is an important intermediate via which the reaction can proceed.

The yielding CH_3COH prefers to be dehydrogenated rather than dissociated. Both C−C and C−O paths are not favored due to the high-energy barriers of 1.11 and 1.27 eV, respectively. In contrast, the dehydrogenation reactions are more plausible, which significantly lowers the barriers by at least 50% relative to the dissociation process. We found that β-dehydrogenation (E_a = 0.48 eV) and hydroxyl dehydrogenation (E_a = 0.61 eV) have comparable energy barriers, thus the reaction pathway is bifurcated at this point. Here, two possibilities are involved: one is started from 1-hydroxyvinyl (CH_2COH) which is generated by β-H elimination of CH_3COH; the other walks along acetyl (CH_3CO), which is formed by hydroxyl dehydrogenation of CH_3COH.

Similarly, the dehydrogenation is preferred for the further reaction of CH_2COH. At this step, the direct decomposition is

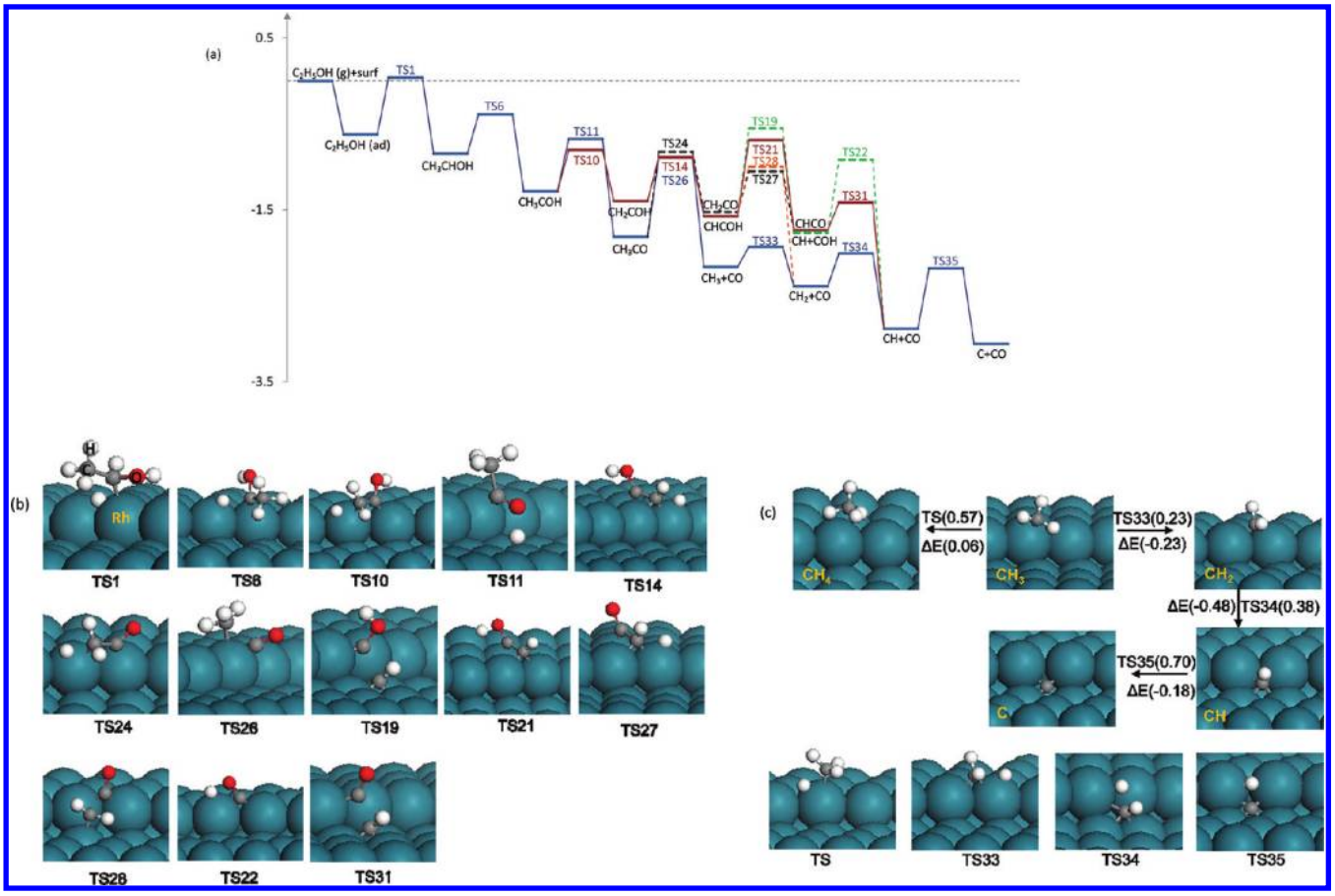

Figure 3. (a) Potential energy diagram for ethanol decomposition on Rh(211). (b) Configurations of transition states involved in (a). (c) Schematics of reaction pathways for CH_3 dehydrogenation and hydrogenation.

still not favored. The barrier for C−C bond breaking is 1.24 eV, which is close to that for C−O bond scission of 1.32 eV. In contrary to the dissociation process of CH_2COH, both of the two distinct dehydrogenation pathways have barriers lower than 1 eV. We noticed that the barrier for C_β−H cleavage of CH_2COH is only 0.51 eV, which is significantly lower than that of O−H breaking by 0.46 eV. Hence, the β-H abstraction to form hydroxyacetylene (CHCOH) is energetically more favorable than the hydroxyl dehydrogenation to produce ketene (CH_2CO). The TS of C_β−H bond breaking is close to the final state (i.e., the optimal configuration of CHCOH), where α-C is located on the off-*t*-top site and β-C is on the *e*-bri site with slightly stretched Rh−C bond distances ($d_{\alpha\text{-C-Rh}}$ =1.983 Å, $d_{\beta\text{-C-Rh}}$ = 2.114, 2.091 Å) as compared to the optimized CHCOH adsorbed system ($d_{\alpha\text{-C-Rh}}$ =1.978 Å, $d_{\beta\text{-C-Rh}}$ = 2.083, 2.043 Å). As shown in Figure 2, the further decomposition of CHCOH is not facile via C_β-H or C−O bond cleavage due to the sizable barriers ($E_{a(C-H)}$ =1.22 eV and $E_{a(C-O)}$ = 2.04 eV). However, the reaction is possible to proceed by breaking the O−H bond (E_a = 0.88 eV) or directly dissociating the C−C bond to form CH and COH species (E_a = 1.02 eV). Subsequently, the CHCO produced via the O−H path undergoes further decarbonylation, which has a lower barrier of 0.32 eV as compared to dehydrogenation (E_a = 0.69 eV) and deoxygenation (E_a = 2.19 eV). On the other hand, for the C−C path, the subsequent dehydrogenation of COH leads to CO and H on the Rh(211) surface. The lower barrier of 0.85 eV reveals that the O−H scission is obviously superior to the C−O bond breaking in COH (E_a = 1.10 eV).

As for another possible dehydrogenation product of CH_3COH, the reactions of CH_3CO have also been studied. By comparing energy barriers of diverse pathways, we found the further reaction of CH_3CO can proceed either by removing H in the hydroxyl group to form ketene (CH_2CO) or by the C−C dissociation to produce methyl (CH_3) and CO. Additionally, the C−O breaking path has been ruled out due to the relative high barriers of 1.12 eV. We noticed that the dehydrogenation and decarbonylation process have quite similar energy barriers with the E_a difference of 0.07 eV, and the C−C breaking path (E_a = 0.92 eV) is slightly more favorable. Actually, which reaction sequence is followed, direct methyl or hydrogen elimination, largely depends on the metal identity and surface structure. On Pd(111),[27] experiments demonstrated that the acetyl species is prone to eliminating H to form a ketene species; however, on Pd(110)[25] and Rh(111) surfaces,[7] the presence of a kinetic isotope effect indicated that C−C instead of C−H scission is a key step in the decarbonylation process, and thus the direct elimination of the methyl group can be observed. In addition, the previous DFT calculations indicated that both Pt(111) and Pt(211) surfaces have preference to form active ketene rather than a methyl group in the sequential reactions of acetyl species.[26] At present, the preferred sequence is still ambiguous for the Rh(211) surface, thus both reaction channels are considered.

For the CH_2CO intermediate, the C−O scission is the most unlikely reaction path. The strong C−O double bond leads to a

dx.doi.org/10.1021/jp206837z |*J. Phys. Chem. C* 2011, 115, 22429–22437

high barrier (E_a =1.18 eV) for C−O dissociation. Other than the C−O path, both the H and methylene (CH_2) elimination are more facile as compared to the previous step (the dissociation of CH_3CO). As depicted in Figure 2, C−H and C−C bonds breaking are competing dissociation channels, and the barriers are 0.47 and 0.53 eV, respectively. However, previous studies on dissociation reactions of CH_2CO on Rh(111) indicated that the barrier for the C−C dissociation is 1.06 eV (24.5 kcal/mol), which is significantly higher than that for the H removal (E_a = 0.51 eV, i.e., 11.7 kcal/mol).[13] Comparing the literature data and the present work, it can be seen that the Rh-step in the Rh(211) surface has the advantage of a breaking C−C bond, and the energy barrier has been importantly reduced to 0.53 eV. This is consistent with the general trend that the defect surface with lower coordinate number is more active than the perfect surface.[21,30] Apart from the decarbonylation, the reaction is likely to proceed via the formation of the CHCO intermediate, which subsequently undergoes C−C cleavage, depositing CH and CO moieties at the Rh-step as we discussed above.

Another possible product of CH_3CO dissociation is the methyl group (CH_3). Several DFT calculations have been performed to study dehydrogenation and hydrogenation possibilities for CH_x species on Rh(111).[13,14,36] Li et al. reported that CH_x species tend to be progressively dehydrogenated to reach complete decomposition; contradictorily, Choi and Liu carried out microkinetic modeling and argued that the high H coverage under typical experimental conditions will overpass the small barrier difference (0.05 eV) between dehydrogenation and reverse the process and thus facilitate the methylene hydrogenation. To get a picture on the Rh(211) surface, we investigated all reactions starting from CH_3. As shown in Figure 3 (c), there are two possible channels: (1) undergo hydrogenation to form methane and (2) walk along the dehydrogenation route as $CH_3 \rightarrow CH_2 \rightarrow CH \rightarrow C$. According to our calculations, the hydrogenation of CH_3 has an energy barrier of 0.57 eV ($CH_3 + H \rightarrow CH_4$ is slightly endothermic with ΔE = 63 meV), whereas the barrier for H abstraction is only 0.23 eV. It seems that the lower activation energy facilitates the stepwise methyl dehydrogenation rather than the reverse process on Rh(211). In Figure 3(c), we can see that the overall dehydrogenation process is exothermic, and the step $CH_2 \rightarrow CH + H$ has the largest energy decrease of 0.48 eV. In the course of sequential H removal, it can be seen that the first methyl activation step is easiest ($CH_3 \rightarrow CH_2 + H$, E_a = 0.23 eV), followed by H elimination from CH_2 (0.38 eV); however, the CH dehydrogenation has the highest energy barrier of 0.70 eV. We found that all the transition states are late-type, which resembles the dissociation behavior of methyl on the Rh(111) surface.[14,42]

3.3. Potential Energy Diagram of Ethanol Decomposition. As shown in Figure 3(a), the energy profile of ethanol decomposition on Rh(211) has been built in this work. The total energy of gas ethanol plus clean surface is set to zero, and all other energies including energies for initial states, transition states, intermediate states, and final states refer to this value.

It can be seen that the reaction starts with α-H elimination to produce CH_3CHOH. The adsorption of CH_3CHOH is more exothermic compared to CH_3CH_2OH with the reaction energy of −0.22 eV. Sequentially, the second H is easily dehydrogenating at the α-C site again with the barrier of 0.46 eV and reaction enthalpy of −0.44 eV. Starting from CH_3COH, the decomposition has two possibilities: C_β−H breaking (red path) or O−H breaking (blue path). Although the barrier difference in dehydrogenation at the β-C site and at the hydroxyl group is only 0.13 eV, the production energies (CH_2COH and CH_3CO) are quite different. We can see that the adsorption system of CH_3CO on the Rh step is thermodynamically more stable than that of CH_2COH. Producing CH_3CO via CH_3COH is a typical exothermic reaction with the reaction energy of −0.53 eV, whereas the C_β−H bond-breaking reaction of CH_3COH is almost thermoneutral (ΔE = −0.11 eV), which is similar to the thermodynamics of the same bond breaking on the Pt surface.[26] Looking at the pathway via CH_2COH (red), we found that the further β-dehydrogenation is facile; however, the reaction is slowed down by the sequential hydroxyl dehydrogenation (TS21, 0.88 eV) or decarbonylation (TS19, 1.02 eV). As shown in Figure 3 (a), it can be seen that regardless of breaking the O−H or C−C bond in CHCOH the energy barrier is always higher than the corresponding previous step (TS14) and following step (TS31and TS22, respectively). Although the two decomposition routes starting from CHCOH, including O−H bond breaking followed by C−C cleavage (red, abbreviated as [O−H plus C−C]) and the reverse sequence, i.e., C−C cleavage followed by O−H bond breaking (green, abbreviated as [C−C plus O−H]), have very similar reaction energies, the magnitude of the reaction barrier obviously depends on the order of bond cleavage. It is clear that the [C−C plus O−H] path is ruled out due to its sizable barriers, and thus one of the possible reaction pathways is $CH_3CH_2OH \rightarrow CH_3CHOH \rightarrow CH_3COH \rightarrow CH_2COH \rightarrow CHCOH \rightarrow CHCO \rightarrow CH + CO \rightarrow C + CO$, which is the red path in Figure 3(a). On the red path, the key reaction step is the hydroxyl dehydrogenation of CHCOH to produce CHCO.

Observing the reaction pathway with CH_3CO as an intermediate (blue), we noticed that the further decarbonylation of CH_3CO is an exothermic reaction with the reaction energy of −0.35 eV (blue); in contrast, the dehydrogenation process is endothermic, and the product ($CH_2CO + H$) is less stable than the reactant of CH_3CO by 0.24 eV (black). Judging from reaction barriers, the H elimination and methyl elimination are competing processes due to the negligible barrier difference (0.07 eV), and the latter is slightly more preferred. The produced CH_2CO can be directly decarbonylated to get CH_2 and CO (orange). Alternatively, it undergoes sequential C−H and C−C bond cleavage to generate CH and CO species (black). From our presented results, we found that starting from CH_3CO onward, whichever reaction pathway is chosen, CH_x species and CO will be produced in the end. That is, the complicated decomposition course of ethanol on the Rh(211) surface will end with the dehydrogenation of the CH_x species. As we discussed above, the progressive dehydrogenation of CH_3 is more favorable than the hydrogenation to produce methane, and the H removal from CH_3 has a low energy barrier of 0.23 eV, which is more facile than both dehydrogenation and decarbonylation of CH_2CO (E_a = 0.47 and 0.53 eV, respectively). Thus, the paths of $CH_3CO \rightarrow CH_2CO \rightarrow CHCO$ and $CH_3CO \rightarrow CH_2CO \rightarrow CH_2 + CO$ are prohibited. On the basis of our calculations, another likely reaction pathway (blue path) can be depicted as $CH_3CH_2OH \rightarrow CH_3CHOH \rightarrow CH_3COH \rightarrow CH_3CO \rightarrow CH_3 + CO \rightarrow CH_2 + CO \rightarrow CH + CO \rightarrow C + CO$, in which the key step is the decarbonylation of CH_3CO.

By comparing the red path and the blue path, we found that the contributions from both pathways are very similar, and the specific reaction rate will depend on reaction conditions, such as temperature and concentration. Therefore, according to our DFT calculations we proposed that the two possible reaction

pathways, i.e., the red via CH_2COH and the blue via CH_3CO, may exist simultaneously during the ethanol decomposition on the Rh(211) surface. The reaction route bifurcates from CH_3COH, and the α-dehydrogenation of CH_3CH_2OH (TS1) is one of the slow steps.

In terms of the present calculations and available literature on ethanol decomposition on transition metal surfaces, there are several points we would like to discuss here:

(1) CH_3COH is an important intermediate for ethanol decomposition on Rh(211). This is different from the ethanol decomposition behavior on other transition metal surfaces or on the same metal with different facet. For example, on Pt(111) and Pd(111), the reaction proceeds via CH_3CHO; for another example, on Rh(111) an oxametallacycle species is produced by sequentially removing H from the O site and β-C site. Indeed, this kind of relationship between dissociation behavior and surface coordination number can also be observed for other molecules. CO dissociation is one of the extremely important cases. It was found that the stepped Rh(211) surface[30,43] and Rh nanopyramids[44] with undercoordinated edges have high reactivity to break the C−O bond, which otherwise remains intact on the flat terrace.

(2) Both experimental findings[7,45] and theoretical calculations[12,13] indicated that the final products of ethanol decomposition on Rh(111) are C and CO. Further mechanistic studies claimed that the C contamination is the major obstacle for ethanol oxidation on Rh(111) due to the strong C−Rh interaction.[12,13] On the Rh(111) surface, it was reported that the activation energy for CH → C + H is 1.16 eV[12] (1.06 eV (24 kcal/mol)[13]), and the C atom is exothermically adsorbed on the hcp site with E_{ad} of −7.79 eV[12] (−7.13 eV[39], −6.8 eV (−156.8 kcal/mol)[13]). However, considering the Rh(211) surface, the step is more active than the (111) terrace, and thus the lower dissociation energy barrier and stronger C−Rh interaction are expected in this work. On the basis of our calculations, we found that the most stable chemisorption site for the C atom is the *s*-hollow site at step (K in Figure 1), and the adsorption energy is improved to −8.03 eV. In addition, the C−H bond is broken at the Rh(211) step and the transition state close to the final state with a lower barrier of 0.70 eV as compared to the Rh(111) surface. Compared to previous findings on Rh(111), we noted that the deactivation of Rh catalyst caused by residual C is probably more serious on Rh(211). The addition of second metal atoms into the Rh matrix is a feasible means to weaken the interaction between the C and Rh surface. Choi and Liu have built a simplified (111) surface model to explore the influence of Rh−Pt and Rh−Pd alloys on C−Rh bond strength and found that the presence of Pt and Pd makes C removal easier.[12]

(3) The mechanistic studies on ethanol decomposition can provide some clues to the understanding of the ethanol steam reforming to produce H_2. In the present work, the water effect on the reaction is not involved. However, indeed, H_2O is an indispensable factor in real steam reforming reactions and plays an important role in determining the entire reaction mechanism. The hydroxyl group in H_2O will interact strongly with CH_3CH_2OH by a H-bond effect, and thus it is expected to modify the breaking barrier of the polar bond O−H on the surface.

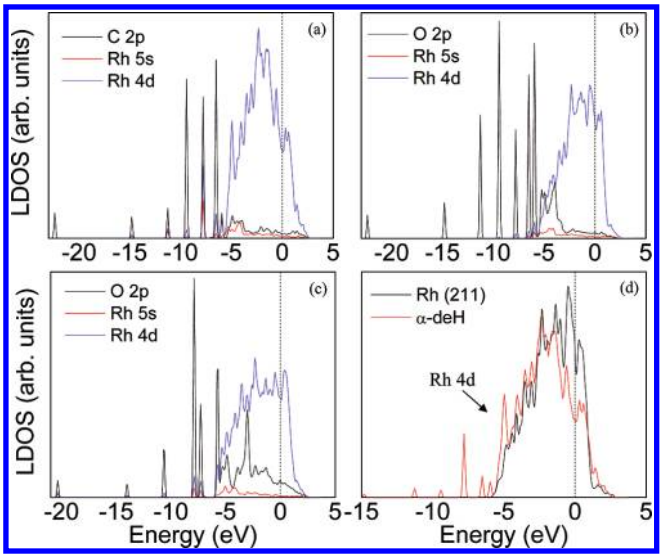

Figure 4. Partial density of states for (a) Rh(211) with the TS complex at α-dehydrogenation and step edge Rh bonding with α-C. (b) Rh(211) with the TS complex at α-dehydrogenation and step-edge Rh bonding with O. (c) Rh(211) with the TS complex at hydroxyl dehydrogenation and step-edge Rh bonding with O. (d) 4d states of the step-edge Rh atom on Rh(211) with and without the TS complex at α-dehydrogenation. The zero energy is the Fermi level.

3.4. Electronic Understanding of the Initial C_α−H vs O−H Path. As we discussed above, the preference of α-dehydrogenation or hydroxyl dehydrogenation in ethanol depends on the facet of the Rh surface. To understand the physics behind the surface-sensitivity for the reaction pathway, we investigated electronic structures in the transition states for the initial C_α−H and O−H bond breaking of ethanol on Rh(211) and Rh(111) surfaces. In Figure 4, we presented the partial electronic density of states (PDOS) projected onto α-C, O and surface Rh bonding to these atoms, where the Fermi level is taken as the zero of energy. It can be seen that the coupling to s electrons of Rh leads to a broadening of 2p states in adsorbates and the coupling to d electrons resulting in bonding and antibonding states.[46] In the case of the transition state for C_α−H cleavage on Rh(211), the 2p orbitals of C interact with d-orbitals of the surface Rh to form bonding states around −5 eV and antibonding states above the Fermi level. Apart from the C atom, the 2p states of O also overlap with d-states of the Rh atom at −5 eV, suggesting that O is involved in TS−surface bonding via p−d coupling, which agree with the TS structure for C_α−H cleavage depicted above. For the TS of O−H cleavage, the O−H bond breaking at the Rh(211) step, where O and H interact with the edge and the lower-edge Rh atoms, respectively (see dotted white line in Figure 1). According to our PDOS calculations, the 2p states arising from O are located in a wide energy range, and a large proportion of mixing states between p orbitals of O and d orbitals of Rh occur between −6 eV and the Fermi level. In Figure 4(d), we show the surface Rh 4d states for Rh(211) with and without the TS-complex of C_α−H bond breaking. It can be seen that d-electrons decrease around the Fermi level and increase in the lower-energy region. Again, some new peaks appear at low-energy levels, ranging from −6 to −12 eV. As a consequence, the d-band of the Rh atom is shifted downward relative to the Fermi

Table 2. Decomposition of the TS Chemisorption Energy (E^{TS}) of $C_2H_5OH- > CH_3CHOH + H$ and $C_2H_5OH- > CH_3CH_2O + H$ on Rh(111) and Rh(211) Surfaces

	$E_{CH3CHOH}{}^{TS}$ (eV)	$E_H{}^{TS}$ (eV)	$E_{geo}{}^{TS}$ (eV)	E^{TS} (eV)	$E_{CH3CH2O}{}^{TS}$ (eV)	$E_H{}^{TS}$ (eV)	$E_{geo}{}^{TS}$ (eV)	E^{TS} (eV)
Rh(111)	1.35	2.49	0.17	3.67	1.89	2.61	0.27	4.23
Rh(211)	1.91	2.40	0.10	4.21	2.12	2.52	0.23	4.41

level due to the TS−surface interaction. On Rh(111) surfaces, the transition states have electronic structures (see Figure S3 in Supporting Information) similar to those on Rh(211).

To quantify the variation of d-band, we calculate the energy of d-states (E_d) in the presence/absence of the TS complex (E_d^{TS} and E_d^{clean}), which reflects the electron contribution to the total energy. Integrating the normalized d-projected density of states of the surface Rh atom according to eq 1,[26] the d-electron energy can be obtained.

$$E_d = \int_{-\infty}^{E_f} n_d \varepsilon d\varepsilon \quad (1)$$

In eq 1, ε is the eigenvalue. Furthermore, the stabilization energy of d-states at the TS is defined as $\Delta E_d = E_d^{TS} - E_d^{clean}$.[26] On the basis of our calculations, the ΔE_d is −3.23 eV for α-dehydrogenation and −3.65 eV for hydroxyl dehydrogenation on Rh(111), whereas the stabilization energy of d-states changed to −4.92 and −4.56 eV, respectively, on Rh(211). It can be seen that (i) the step-edge Rh atom on Rh(211) is more active than the one on Rh(111). The calculated E_d^{clean} for step-edge Rh is −14.60 eV; however, the value for the atom on Rh(111) is −15.69 eV. The relatively higher d-state energy of Rh(211) directly leads to the stronger TS complex−surface interaction. (ii) On the Rh(111) surface, the hydroxyl dehydrogenation (ΔE_d = −3.65 eV) stabilizes the d-states more than the α-dyhydrogenation (ΔE_d = −3.23 eV); however, the order is reversed for the Rh(211) surface (ΔE_d = −4.56 eV for the O−H path and −4.92 eV for α-H removal). In fact, at the TS for the α-dehydrogenation reaction on Rh(211), not only C_α and α-H but also O have a relatively strong interaction with the Rh surface (d_{O-Rh} = 2.365 Å and d_{O-Rh} = 2.960 Å at TS1 on Rh(211) and Rh(111), respectively). The O−Rh bonding stabilizing the d-electron energy by 0.62 eV (ΔE_d), together with the contributions coming from C_α and α-H (ΔE_d = −4.30 eV) results in a more stable TS for α-dehydrogenation (ΔE_d = −4.92 eV). As a consequence, the preference of the C_α−H path in the first step of ethanol decomposition on Rh(211) can be observed.

We further decomposed the chemisorptions energy of the TS (E^{TS}) into an electronic component and geometric component according to ref 30. The E^{TS} can be expressed as $E^{TS} = E_A{}^{TS} + E_H{}^{TS} - E_{geo}{}^{TS}$ (A = CH_3CHOH, CH_3CH_2O), where $E_A{}^{TS}$ and $E_H{}^{TS}$ are respective chemisorption energies at TS configurations (electronic component); also the remainder of the interaction energy between A and H at TS is defined as $E_{geo}{}^{TS}$ (geometric component). As shown in Table 2, the decrease of the barrier for the α-dehydrogenation reaction on step surface is mainly due to the increase of the electronic component. It can be seen that the $E_{CH_3CHOH}{}^{TS} + E_H{}^{TS}$ is enhanced by 0.47 eV from the flat to the step surface, which is favorable to the decrease of the energy barrier; however, the $E_{geo}{}^{TS}$ hardly changes (0.07 eV). Similarly, for the O−H path the contribution of $E_{geo}{}^{TS}$ to the change of E^{TS} is trivial (0.04 eV). Thus, local electronic effect is a dominant factor resulting in the barrier variation of the dehydrogenation course on Rh(211), which can be largely reflected by the stabilization energy of d-states (ΔE_d) at transition states.

4. CONCLUSION

The adsorption and decomposition of ethanol on the Rh(211) surface have been investigated using DFT calculations. Results show that ethanol and most ethanol-derived species always prefer to adsorb on step-edge sites. In addition, the most stable adsorption site moves from *e*-top to *e*-bridge and then to hollow site with the increase of C valency. The mechanistic studies indicated that the decomposition reaction initially proceeds via progressive α-dehydrogenation to CH_3COH, from which the reaction path is bifurcated. The two parallel paths undergo direct decarbonylation to get the CH_x (x = 1 and 3) group and CO adsorbed at the surface step. Subsequently, the further CH_x dissociation leads to final products C and CO. The residue C may cause more serious catalyst deactivation as compared to the Rh(111) surface due to the stronger C−Rh interaction on the Rh(211) surface. In this work, the detailed ethanol decomposition mechanism on Rh(211) has been first proposed, which will shed some light on ethanol steam reforming and electrooxidation.

■ ASSOCIATED CONTENT

Supporting Information. Figures S1−S3 and Tables S1 and S2. This material is available free of charge via the Internet at http://pubs.acs.org.

■ AUTHOR INFORMATION

Corresponding Author

*E-mail: wuping@ihpc.a-star.edu.sg; wuping@sutd.edu.sg.

Present Addresses

⊥Singapore University of Technology and Design, 20 Dover Drive, Singapore 138682

■ ACKNOWLEDGMENT

Jia Zhang would like to thank Dr. Quek Su Ying from IHPC for helpful discussions.

■ REFERENCES

(1) Ni, M.; Leung, Y. C.; Leung, M. K. H. *Int. J. Hydrogen. Energy* **2007**, *32*, 3238.
(2) Haryanto, A.; Ferando, S.; Murali, N.; Adhikari, S. *Energy Feuls* **2005**, *19*, 2098.
(3) Zhong, Z.; Anr, H.; Choong, C.; Chen, L.; Huang, L.; Lin, J. *Phys. Chem. Chem. Phys.* **2009**, *11*, 872.
(4) Besenbacher, F.; Chorkendorff, I.; Clausen, B. S.; Hammer, B.; Molenbroek, A. M.; Nørskov, J. K.; Stensgaard, I. *Science* **1998**, *279*, 1913.
(5) Alcalá, R.; Mavrikakis, M.; Dumesic, J. A. *J. Catal.* **2003**, *218*, 178.
(6) Davis, J. L.; Barteau, M. A. *Surf. Sci.* **1990**, *235*, 235.

(7) Houtman, C. J.; Barteau, M. A. *J. Catal.* **1991**, *130*, 528.
(8) Vesselli, E.; Baraldi, A.; Comelli, G.; Lizzit, S.; Rosei, R. *ChemPhysChem* **2004**, *5*, 1133.
(9) Xu, J.; Zhang, X.; Zenobi, R.; Yoshinobu, J.; Xu, Z.; Yates, J. T., Jr. *Surf. Sci.* **1991**, *256*, 288.
(10) Lee, A. F.; Gawthrope, D. E.; Hart, N. J.; Wilson, K. *Surf. Sci.* **2004**, *548*, 200.
(11) Mavrikakis, M.; Barteau, M. A. *J. Mol. Catal A: Chem.* **1998**, *131*, 135.
(12) Choi, Y. M.; Liu, P. *Catal. Today* **2011**, *165*, 64.
(13) Li, M.; Guo, W.; Jiang, R.; Zhao, L.; Lu, X.; Zhu, H.; Fu, D.; Shan, H. *J. Phys. Chem. C* **2010**, *114*, 21493.
(14) Wang, J.-H.; Lee, C. S.; Lin, M. C. *J. Phys. Chem. C* **2009**, *113*, 6681.
(15) Sheng, P. Y.; Idriss, H. *J. Vac. Sci. Technol. A* **2004**, *22*, 1652.
(16) Sheng, P.-Y.; Yee, A.; Bowmaker, G. A.; Idriss, H. *J. Catal.* **2002**, *208*, 393.
(17) Kowal, A.; Li, M.; Shao, M.; Sasaki, K.; Vukmirovic, M. B.; Zhang, J.; Marinkovic, N. S.; Liu, P.; Frenkel, A. I.; Adzic, R. R. *Nat. Mater.* **2009**, *8*, 325.
(18) Idriss, H. *Platinum Metals Rev.* **2004**, *48*, 105.
(19) Kugai, J.; Velu, S.; Song, C. *Catal. Lett.* **2005**, *101*, 255.
(20) Cong, Y.; Spaendonk, V. V.; Masel, R. I. *Surf. Sci.* **1997**, *385*, 246.
(21) Tarnowski, D. J.; Korzeniewski, C. *J. Phys. Chem. B* **1997**, *101*, 253.
(22) Shin, J.; Tornquist, W. J.; Korzeniewski, C.; Hoaglund, C. S. *Surf. Sci.* **1996**, *364*, 122.
(23) Souza-Garcia, J.; Herrero, E.; Feliu, J. M. *ChemPhysChem* **2010**, *11*, 1391.
(24) Lai, S. C. S.; Koper, M. T. M. *J. Phys. Chem. Lett.* **2010**, *1*, 1122.
(25) Bowker, M.; Holroyd, R. P.; Dharpe, R. G.; Corneille, J. S.; Francis, S. M.; Goodman, D. W. *Surf. Sci.* **1997**, *370*, 113.
(26) Wang, H.-F.; Liu, Z.-P. *J. Am. Chem. Soc.* **2008**, *130*, 10996.
(27) Davis, J. L.; Barteau, M. A. *J. Am. Chem. Soc.* **1989**, *111*, 1782.
(28) Resta, A.; Gustafson, J.; Westerström, R.; Mikkelsen, A.; Lundgren, E.; Andersen, J. N.; Yang, M.-M.; Ma, .-F.; Bao, X.-H.; Li, W.-X. *Surf. Sci.* **2008**, *602*, 3057.
(29) Zamvelli, T.; Wintterlin, J.; Throst, J.; Ertl, G. *Science* **1996**, *273*, 1688.
(30) Liu, Z.-P.; Hu, P. *J. Am. Chem. Soc.* **2003**, *125*, 1958.
(31) Kresse, G.; Hafner, J. *Phys. Rev. B* **1993**, *48*, 13115. *Phys. Rev. B* **1994**, *49*, 14251.
(32) Bloechl, P. E. *Phys. Rev. B* **1994**, *50*, 17953.
(33) Kresse, G.; Joubert, D. *Phys. Rev. B* **1999**, *59*, 1758.
(34) Perdew, J. P.; Wang, Y. *Phys. Rev. B* **1992**, *45*, 13244.
(35) *CRC handbook of Chemistry and Physics*, 76th ed.; Lide, D. R., Ed.; CRC Press: New York, 1996.
(36) Choi, Y. M.; Liu, P. *J. Am. Chem. Soc.* **2009**, *131*, 13054.
(37) Alavi, A.; Hu, P.; Deutsch, T.; Silvestrelli, P. L.; Hutterm, J. *Phys. Rev. Lett.* **1998**, *80*, 3650.
(38) *CRC handbook of Chemistry and Physics*, 3rd electronic ed.; Lide, D. R., Ed.; CRC Press: Boca Raton, FL, 2000.
(39) Kapur, N.; Hyun, J.; Shan, B.; Nicholas, J. B.; Cho, K. *J. Phys. Chem. C* **2010**, *114*, 10171.
(40) Yang, M.-M.; Bao, X. H.; Li, W.-X. *J. Phys. Chem. C* **2007**, *111*, 7403.
(41) Wang, H.-F.; Liu, Z.-P. *J. Phys. Chem. C* **2007**, *111*, 12157.
(42) Bunnik, B. S.; Kramer, G. J. *J. Catal.* **2006**, *242*, 309.
(43) Mavrikakis, M.; Bäumer, M.; Freund, H.-J.; Nørskov, J. K. *Catal. Lett.* **2002**, *81*, 153.
(44) Buatier de Mongeot, F.; Toma, A.; Molle, A.; Lizzit, S.; Petaccia, L.; Baraldi, A. *Phys. Rev. Lett.* **2006**, *97*, 056103.
(45) Papageorgopoulos, D. C.; Ge, Q.; King, D. A. *J. Phys. Chem.* **1995**, *99*, 17645.
(46) Hammer, B.; Nørskov, J. K. *Adv. Catal.* **2000**, *45*, 71.